Rapid Communications

Production of relativistic electrons at subrelativistic laser intensities

G. J. Williams,[1] A. Link,[1] M. Sherlock,[1] D. A. Alessi,[1] M. Bowers,[1] A. Conder,[1,*] P. Di Nicola,[1] G. Fiksel,[2] F. Fiuza,[3] M. Hamamoto,[1] M. R. Hermann,[1] S. Herriot,[1] D. Homoelle,[1] W. Hsing,[1] E. d'Humières,[4] D. Kalantar,[1] A. Kemp,[1] S. Kerr,[1] J. Kim,[5] K. N. LaFortune,[1,*] J. Lawson,[1,†] R. Lowe-Webb,[1] T. Ma,[1] D. A. Mariscal,[1] D. Martinez,[1] M. J.-E. Manuel,[6] M. Nakai,[7] L. Pelz,[1] M. Prantil,[1] B. Remington,[1] R. Sigurdsson,[1] C. Widmayer,[1] W. Williams,[1] L. Willingale,[2] R. Zacharias,[1] K. Youngblood,[6] and Hui Chen[1]

[1]*Lawrence Livermore National Laboratory, Livermore, California 94550, USA*
[2]*Center for Ultrafast Optical Science, University of Michigan, Ann Arbor, Michigan 48109, USA*
[3]*High Energy Density Science Division, SLAC National Accelerator Laboratory, Menlo Park, California 94025, USA*
[4]*CELIA, Université de Bordeaux, Talence, France*
[5]*Center for Energy Research, University of California, San Diego, California 92093, USA*
[6]*General Atomics, San Diego, California 92186, USA*
[7]*Institute of Laser Engineering, Osaka University, 2-6 Yamadaoka, Suita, Osaka 565-0871, Japan*

(Received 18 March 2019; revised manuscript received 2 August 2019; accepted 6 February 2020; published 4 March 2020)

Relativistic electron temperatures were measured from kilojoule, subrelativistic laser-plasma interactions. Experiments show an order of magnitude higher temperatures than expected from a ponderomotive scaling, where temperatures of up to 2.2 MeV were generated using an intensity of 1×10^{18} W/cm^2. Two-dimensional particle-in-cell simulations suggest that electrons gain superponderomotive energies by stochastic acceleration as they sample a large area of rapidly changing laser phase. We demonstrate that such high temperatures are possible from subrelativistic intensities by using lasers with long pulse durations and large spatial scales.

DOI: 10.1103/PhysRevE.101.031201

Experimental and theoretical studies in the past decades on laser-solid interactions at relativistic intensities ($I_L > 10^{18}$ W/cm^2 for $\lambda \sim 1$ μm) have established that electrons can be generated with energies of tens of MeV at high efficiencies [1–6]. These electrons provide the energy for the production of secondary sources such as x rays [7,8], ions [9,10], neutrons [11,12], and positrons [13]. Understanding electron acceleration in all laser regimes is critical to applications based on laser-driven sources for scaled experiments that study astrophysical phenomenon [14], compressed heated material [15,16], and high-energy-density conditions [17].

The mechanisms responsible for laser fields accelerating electrons to relativistic energies are highly sensitive to plasma conditions and laser intensity. For interactions with steep plasma density profiles, the dominant energy transfer mechanism is $\mathbf{j} \times \mathbf{B}$ heating [1,2]. In the presence of plasma densities less than critical ($n_c \approx 10^{-21}$ cm^{-3}), simulations predict that electrons can gain energy by dephasing from a relativistic-intensity laser field [18–25]. The processes by which electrons dephase from the laser, however, are not well understood at subrelativistic intensities.

In recent years, large-scale short-pulse laser facilities have become available [26–29]. Of particular interest is the newly commissioned Advanced Radiographic Capability (ARC) laser [29] at the National Ignition Facility (NIF) [30], which provides a novel diagnostic to NIF experimental platforms. The ARC is unique as the highest-energy short-pulse laser and is a source for high-flux, moderate-energy x-ray radiography [31,32]; however, peak intensities are only marginally relativistic due to the large spot size and long focal length of the final optics. Previous experiments have hinted that electron temperatures exceeding ponderomotive scaling [33–35] may be possible at relatively low intensities. However, questions remain as to the exact mechanism responsible for these observations and whether one can take advantage of the high energies at ARC to generate spectra which have applications normally associated with relativistic intensity lasers. For example, proton radiography or isochoric heating applications conservatively require electron temperatures of ~2 MeV and tens of joules of protons [36]. Positron-electron pair creation becomes efficient for electron temperatures of ~4 MeV with high-energy laser platforms capable of generating a charge neutral plasma with pair yields above 10^{14} [37,38].

In this Rapid Communication, we report on experiments performed using the ARC laser in which the electron spectra, temperature scaling, and conversion efficiencies were measured. We find that subrelativistic laser intensities can be used to generate electrons with relativistic temperatures more than ten times higher than ponderomotive scaling predictions suggest. Two-dimensional (2D) particle-in-cell (PIC) simulations highlight the importance of numerous filamentations in intensity and density that initiate stochastic acceleration responsible for such high temperatures. Previous simulation work has suggested efficient superponderomotive electron

[*]Present address: LCLS, SLAC National Accelerator Laboratory, Menlo Park, California 94025, USA.
[†]Present address: Special Technologies Laboratory, Santa Barbara, California 93111, USA.

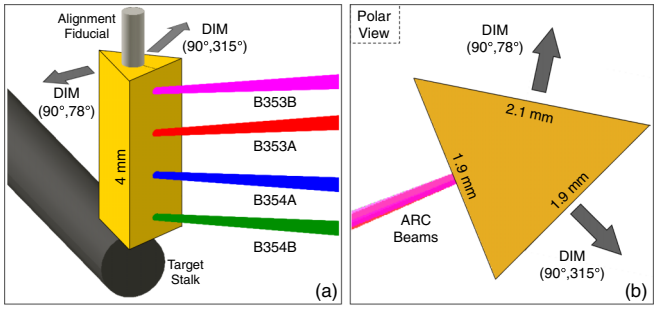

FIG. 1. (a) Diagram of the experimental setup with ARC beamlets incident on a gold prism target. (b) Polar view of the target.

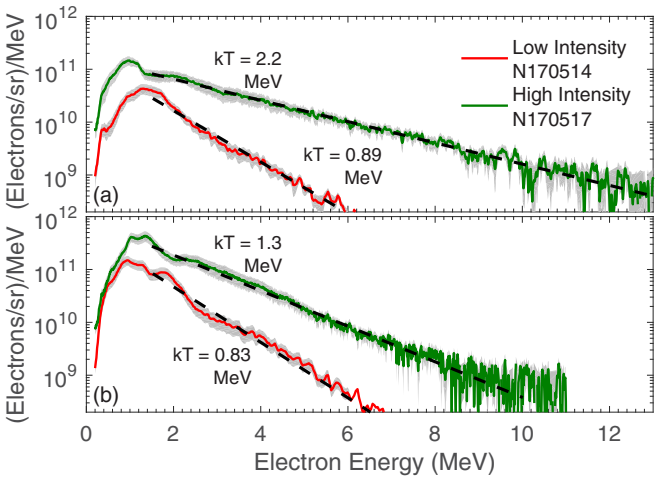

FIG. 2. Electron measurements from $(90°, 78°)$ (a) and $(90°, 315°)$ (b) viewing angles. 1σ error bounds are shown in shaded regions. Dashed lines are single-exponential temperature fits between 1.5 MeV and the detection limit.

acceleration is possible at relativistic intensities; however, we demonstrate this is also possible at lower intensities when the pulse length is long and the spot size is sufficiently large. Two experiments were performed that varied laser intensity to observe a change in accelerated electron temperature, where MeV temperatures were measured at nominal on-target intensities of $I_L \leqslant 10^{18}$ W/cm^2. The results presented here provide insight into electron acceleration mechanisms at large spatial and temporal scales.

A model of the target and diagnostic orientation is shown in Fig. 1, where the laser angle of incidence onto an Au target was between 10° and 15° for each of the four ARC beamlets (see the Supplemental Material for additional details of the experimental geometry and laser parameters [39]). The target rear surfaces are directed towards the equatorial diagnostic instrumentation manipulator (DIM) lines of sight at $(90°, 78°)$ and $(90°, 315°)$, which hold the primary particle diagnostics. This created a prism-shaped target where charged particles were directed towards the DIMs by target normal sheath acceleration (TNSA). Four ARC beamlets, synchronously timed, were spatially separated by 1 mm for each experiment in order to avoid uncertain overlap between beamlet spots. As a result, the overall signal was interpreted as equivalent to the sum of four single beamlets.

Two experiments (NIF shot IDs N170514-002 and N170517-003) were performed with a nominal energy per beamlet of 150 and 600 J at 10 ps pulse duration, which provided a relative low (4×10^{17} W/cm^2) and high (1×10^{18} W/cm^2) intensity interaction, respectively. ARC is a fundamental wavelength laser operating at $\lambda = 1053$ nm. Measurements of the on-shot energy, spectrum, prepulse, and pulse duration were recorded for one of the beamlets. Beamlet foci are elliptically shaped spots with minor and major axes of ∼15 and ∼38 μm full width at half maximum (FWHM), respectively, and contain 30% of the total beam energy. The one-dimensional (1D) equivalent is a 26-μm spot. Here, we reference the peak intensity for simplicity and as a comparison to previous works. The propagated error in the laser parameter calculations conservatively suggests an uncertainty in peak intensity of 50%. The prepulse energy contrast was measured on-shot to be greater than 10^{-8} up to 0.5 ns before the main pulse.

Two NIF electron-positron-proton spectrometers [40] (NEPPS) measured energetic electrons and protons from two equatorial DIMs at a standoff of 56 cm each. The high-intensity experiment used a copper step filter in the $(0°, 0°)$ direction to measure the spectrum of x rays emitted from the target.

Electron acceleration was quantified by measuring the spectral slope to determine a characteristic temperature for each experiment. Electron spectra collected by each NEPPS are shown in Fig. 2. An exponential fit to the high-energy region of each spectrum was performed between 1.5 MeV and the detection threshold of $\sim 5 \times 10^8$ electrons/MeV/sr. The propagated uncertainty in the measurement is shown as a shaded area around the spectra (∼20%). The measured electron temperatures are consistent between the two lines of sight for the low-intensity experiment with 0.89 ± 0.10 and 0.83 ± 0.07 MeV for $(90°, 78°)$ and $(90°, 315°)$, respectively. An asymmetry in flux is observed with approximately three times more signal towards $(90°, 315°)$. This is hypothesized to be due to geometric asymmetries with respect to the laser and the dynamic sheath field evolution that influences the quantity of refluxing electrons. As the collisional mean free path is much less than the target thickness for electrons with energy <10 MeV, most are stopped in the target and the higher-energy electrons experience multiple deflections leading to a wide angular distribution prior to exiting the target. If the electron beam divergence is assumed to be Gaussian with a 2–4 sr (65°–130°) FWHM, the total number of electrons between 1.5 MeV and the detection threshold is estimated to be $(0.76–2.1) \times 10^{12}$ with a total energy of 0.26–0.76 J. This corresponds to a conversion efficiency from laser to escaping high-energy electrons of 0.04%–0.11%.

The high-intensity experiment showed an increase in electron temperatures while retaining the observed asymmetric flux with preference towards the $(90°, 315°)$ direction. The electron temperatures differed between lines of sight where $(90°, 78°)$ observed 2.25 ± 0.35 and 1.34 ± 0.12 MeV in the $(90°, 315°)$ direction. Assuming the same angular divergence, an estimated $(3.8–11) \times 10^{12}$ electrons escaped the target with integrated energies between 1.9 and 5.8 J. The conversion efficiency into MeV electrons increased to 0.08%–0.24%.

Protons with maximum cutoff energies of 3.5 MeV were also observed on this experiment. X-ray bremsstrahlung emission was fit to a single-component exponential with a temperature of 155 ± 30 keV and indicates a strong multitemperature electron profile: a high-flux, colder spectrum at the ponderomotive temperature that stops within the target and a low-flux, hotter spectrum that escapes [41].

The data set obtained at ARC is supplemented by experiments performed at Omega EP [28] using ARC-equivalent laser conditions. Here, the $f/2$ optic was defocused to approximate the ARC spot with 30% of the energy contained in a 25-μm spot. A 5-μm Au foil was irradiated at normal incidence with 550 J of incident laser energy. Pulse duration was scanned between 30, 10, and 3 ps to change the on-target intensity from 0.3, 0.8, and 2.9×10^{18} W/cm^2, respectively. Electron spectra were measured normal to the foil rear surface and analyzed using the same method outlined above. The temperatures derived from the data were found to increase with intensity as 0.73 ± 0.14, 1.76 ± 0.24, and 3.10 ± 0.58 MeV.

Electron temperatures reported here are significantly higher than those expected from acceleration by the laser ponderomotive potential. When a laser interacts with a steep density interface, such that electrons observe only a few cycles of the laser field, PIC calculations [1] predict a Maxwellian electron distribution with a temperature of $kT_{\mathrm{Pond}} = 0.511[(1 + I_{18}\lambda_{\mu\mathrm{m}}^2/1.37)^{1/2} - 1]$ MeV, where I_{18} is the intensity in units of 10^{18} W/cm^2 and $\lambda_{\mu\mathrm{m}}$ is the wavelength in units of micrometers. For the laser intensities considered here, 0.4 and 1.0×10^{18} W/cm^2, $kT_{\mathrm{Pond}} = 0.08$ and 0.18 MeV, respectively. The observed electrons have superponderomotive temperatures that are between 7 times and 12 times higher than the ponderomotive scaling, depending on line of sight and intensity.

Two-dimensional PIC simulations were performed to gain understanding of the acceleration mechanisms responsible for producing the observed electron spectra. The hybrid PIC code Chicago [42] was used to model the laser-plasma interaction of a single ARC beamlet on a surrogate gold target for both the low- and high-intensity cases. These simulations are novel due to the large spatial and temporal scales, with runs of ~0.5 MCPU hours to simulate 40 ps of the interaction. The simulation employed a radial approximation to the ARC laser spot as a superposition of two Gaussian spots of 26 and 120 μm FWHM containing 33% and 67% of the incident energy, respectively, that was delivered in a sin^2 temporal profile with a 10 ps FWHM. Peak vacuum intensities were 0.3 and 1×10^{18} W/cm^2. Simulations were 2D Cartesian and collisions were handled using a cell average Lee-More-Desjarlais collision model [43,44] for thermal electrons (electrons below 25 keV) and Atzeni-Schiavi-Davies collisions [45] for electrons greater than 25 keV. Hard x-ray emission was included inside the solid gold target through an application of the Integrated Tiger Series code [46] which runs inline with the PIC simulation. The simulation box was 400 μm in the transverse dimension and 350 μm along the laser direction with 10 cells per wavelength and 15 steps per optical cycle. The radiation hydrodynamic code HYDRA [47] initialized the preformed plasma profile using measured laser prepulse that provided the initial condition to the PIC simulation. This initial plasma had a scale length of 15.2 μm below critical density, 7.5 μm between n_c and $7n_c$, and 1.3 μm from $7n_c$ to solid density.

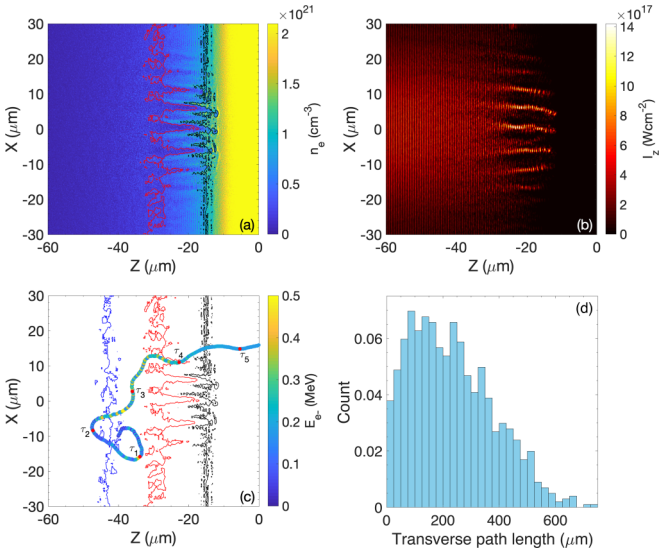

FIG. 3. (a) Electron density at $\tau = -3$ ps with $n_c/4$ and n_c contours drawn in red and black, respectively (peak intensity occurs at $\tau = 0$ ps). (b) Laser intensity at the same time step. (c) Example trajectory of an electron with a two times ponderomotive final energy and $n_c/10$ contour shown in addition to those in (a). Electron motion is incoherent and rapid energy gains occur as it moves transversely across a changing laser phase. 100 fs time steps are labeled. (d) Histogram of transverse path length for electrons with energies above 180 keV.

The PIC simulations show the development of multiple ~3-μm plasma filaments [Fig. 3(a)] close to the quarter-critical surface. The location, magnitude, and size of filaments in our simulations are in agreement with the prior work of Brady *et al.* [48], and as a result, they are attributed to the filamentation instability seeded by Raman scattering. Filaments are found in both plasma density and laser intensity, where both simulation cases show peak intensity was enhanced by a factor of ~4 inside the filaments [see Figs. 3(b) and 4(a)]. However, this intensity increase is not sufficient to explain

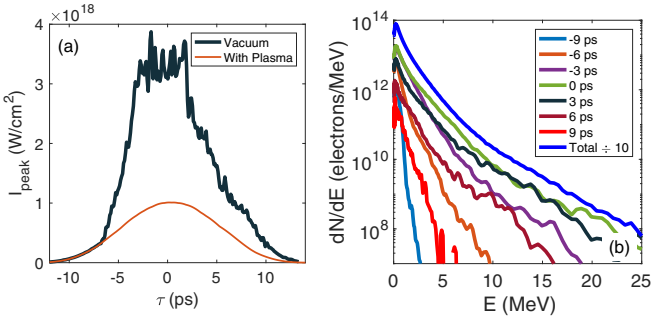

FIG. 4. (a) Input laser intensity (red) for the high-intensity case and cycle-averaged laser intensity on the simulation grid (black). An increase is observed due to self-focusing inside density filaments. Self-focusing occurs in both intensity simulations. (b) Simulated time-integrated and time-resolved (± 0.1 ps) electron spectra for the high-intensity case.

the energetic tail in the electron spectrum by ponderomotive arguments because the measured temperatures are significantly greater than ponderomotive at four times the nominal intensity (0.26–0.55 MeV for the low- and high-intensity cases, respectively). The filaments grow rapidly upon being seeded, reaching nonlinear saturation within 100 fs and will be present within any multipicosecond interaction of sufficient intensity.

Simulations reveal that a majority of the electron energy gain occurs in the coronal region ($z < -30$ μm) away from the strong density filaments and that work on the electrons appears to be done by the laser, rather than self-generated, electric fields. The existence of laser filaments is important because their random nature leads to a reflected wave which itself has significant transverse and longitudinal variations in phase. The stochastic acceleration that is enabled by the presence of filaments has been studied by Nakamura *et al.* [49] and, while an analytic scaling was not possible, simplified Fokker-Planck simulations predicted the generation of an energetic tail at energies well above ponderomotive scaling. There is no evidence of ion channel formation in our conditions that could trap electrons within a filament, as has been observed for significantly higher intensities [3]. Instead, electrons experience rapid, stochastic accelerations as they execute highly nonuniform trajectories in the coronal plasma, crossing regions of significantly different laser phase. A typical superponderomotive electron trajectory, color-coded by energy, is shown in Fig. 3(c). In this way, electrons are able to gain energy over hundreds of microns in the coronal plasma and can easily reach relativistic energies so long as they undergo significant phase change. They are therefore not constrained by one-dimensional energy scaling [49].

This is in comparison to small-spot laser interactions, which typically allow for electrons to travel only $\sim$10 μm in the transverse direction before being ejected from locally higher intensity regions, which ultimately limits the number of stochastic accelerations possible. We find that the vast majority of superponderomotive electrons (defined as those with energy >180 keV) sample many laser filaments while in the corona as indicated by their significant ($\gg$3 μm) transverse path lengths, $\int |v_x| dt$ [see Fig. 3(d)]. A large number of filaments can only be generated when the laser spot size is many times larger than the filament size and the plasma scale length is sufficient to sustain these filaments. This suggests that lasers with subrelativistic intensities that have large focal spots and long pulse durations can more easily generate relativistic electrons. Plasma turbulence could also be responsible for the dephasing, as shown in Ref. [50], but the electromagnetic fields associated with the filaments are typically much greater in magnitude than the electrostatic response and the energy jumps visible in Fig. 3(c) are due primarily to the laser fields.

Simulated electron spectra from the laser-plasma interaction were characterized at an extraction plane 10 μm inside the solid density region to capture the particles which would enter the target. This distribution was revolved assuming axisymmetry to get a three-dimensional (3D) equivalent electron distribution to compare to the experiment. The time-integrated and time-resolved electron distributions are shown in Fig. 4(b) for the high-intensity case and indicate a maximum hot electron temperature of 2.5 MeV for the energy region of 8–20 MeV. Simulations of the low-intensity case showed a high-energy electron tail with a temperature of 0.56 MeV.

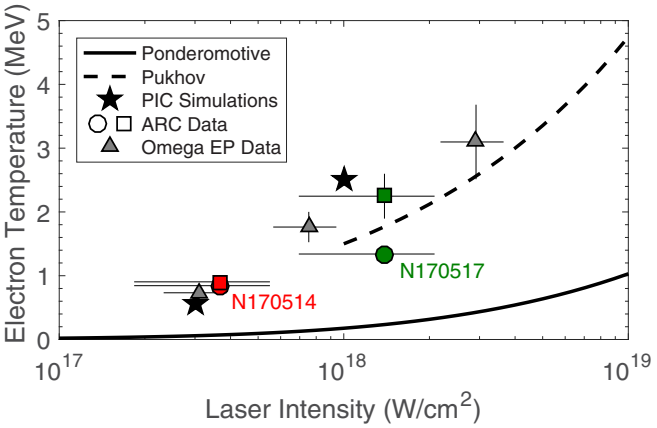

FIG. 5. Measured and simulated electron temperatures. Square and circle markers differentiate ARC data at (90°, 78°) and (90°, 315°) lines of sight, respectively, and are placed at the mean peak intensity of the four beamlets. Horizontal error bars are uncertainty in calculated intensity. For ARC data, error includes scatter in delivered beamlet intensities. Confidence ranges in temperature include uncertainty in measurement and fit. The Pukhov scaling is only shown at intensities considered in their study, above 10^{18} W/cm^2.

We note that the measured electron temperatures appear to agree with the scaling relationship for superponderomotive acceleration described in Pukhov *et al.* [3]. This is despite the fact that the attributed acceleration mechanisms are unique and that we do not observe confining ion channels in our simulations of the kind discussed in Ref. [3]. The ponderomotive and Pukhov scalings are shown in Fig. 5 along with the experimental and simulated electron temperatures as a function of laser intensity.

The simulations show the high-intensity case had a conversion efficiency of 7.8% from laser to electrons above 1.5 MeV at the extraction plane. The conversion efficiency to observable electrons is estimated by injecting the simulated spectrum into a 3D model of the target using the Monte Carlo code GEANT4 [51]. Modeling the dynamic TNSA fields using the PIC code was not tractable due to the large spatial scale and asymmetry of the target that would necessitate a 3D simulation. However, an electric field that develops on the target can be described by a target charging model in the large surface area limit (here, $\sim$1 cm^2) [52]. The protons serve as a measurement of the capacitor charge that downshifts the escaping electrons while the spectrum temperature is maintained. Electrons escaping in the target have their energy reduced by 3.5 MeV and show a conversion efficiency from laser energy to electrons above 1.5 MeV of 0.02%. Angular emission of the scattered electrons created a forward going cone with FWHM of 130°. This agrees with experimental estimates within a factor of 4.

Proton acceleration expected at these laser conditions is estimated using the simulated time-resolved electron spectrum and a 10-μm Au target. 1D PIC simulations of the generated TNSA fields show a maximum proton cutoff energy of $\sim$20 MeV with 30 J of protons produced, sufficient for

radiographic requirements and isochoric heating of materials to tens of eV. Monte Carlo simulations showed the high-intensity experiment generated an emitted positron yield of $\sim 1 \times 10^9$/sr, which was not observed but would have appeared at the detection threshold of the diagnostics. A robust positron signal could be measurable with a doubling of the electron temperature resulting in a yield of 5×10^{10} pairs/sr emitted from the target.

In summary, the first ARC science campaign was completed to measure energetic electrons generated from a subrelativistic laser target interaction. Electrons were observed to have a temperature exceeding 2 MeV, an order of magnitude above the ponderomotive scaling. 2D PIC simulations demonstrated that electrons gain their energy through stochastic accelerations in the coronal plasma as they traverse a large area of rapidly changing laser phase. The results described here establish that highly relativistic electrons can be generated with subrelativistic lasers by using long pulse durations and large spatial scales.

We thank the NIF Experimental Operations team for implementing these experiments. We gratefully acknowledge the NIF Discovery Science Program for the experimental allocation. This work was performed under the auspices of the U.S. Department of Energy by the Lawrence Livermore National Laboratory under Contract No. DE-AC52-07NA27344 and funded by the LLNL LDRD program under tracking code 17-ERD-010.

[1] S. C. Wilks, W. L. Kruer, M. Tabak, and A. B. Langdon, Phys. Rev. Lett. **69**, 1383 (1992).
[2] W. L. Kruer and K. Estabrook, Phys. Fluids **28**, 430 (1985).
[3] A. Pukhov, Z.-M. Sheng, and J. Meyer-ter Vehn, Phys. Plasmas **6**, 2847 (1999).
[4] Y. Ping, R. Shepherd, B. F. Lasinski, M. Tabak, H. Chen, H. K. Chung, K. B. Fournier, S. B. Hansen, A. Kemp, D. A. Liedahl, K. Widmann, S. C. Wilks, W. Rozmus, and M. Sherlock, Phys. Rev. Lett. **100**, 085004 (2008).
[5] A. G. Krygier, D. W. Schumacher, and R. R. Freeman, Phys. Plasmas **21**, 023112 (2014).
[6] J. Peebles, M. S. Wei, A. V. Arefiev, C. McGuffey, R. B. Stephens, W. Theobald, D. Haberberger, L. C. Jarrott, A. Link, H. Chen, H. S. McLean, A. Sorokovikova, S. Krasheninnikov, and F. N. Beg, New J. Phys. **19**, 023008 (2017).
[7] H.-S. Park, N. Izumi, M. H. Key, J. A. Koch, O. L. Landen, P. K. Patel, T. W. Phillips, and B. B. Zhang, Rev. Sci. Instrum. **75**, 4048 (2004).
[8] F. Albert, N. Lemos, J. L. Shaw, B. B. Pollock, C. Goyon, W. Schumaker, A. M. Saunders, K. A. Marsh, A. Pak, J. E. Ralph, J. L. Martins, L. D. Amorim, R. W. Falcone, S. H. Glenzer, J. D. Moody, and C. Joshi, Phys. Rev. Lett. **118**, 134801 (2017).
[9] R. A. Snavely, M. H. Key, S. P. Hatchett, T. E. Cowan, M. Roth, T. W. Phillips, M. A. Stoyer, E. A. Henry, T. C. Sangster, M. S. Singh, S. C. Wilks, A. MacKinnon, A. Offenberger, D. M. Pennington, K. Yasuike, A. B. Langdon, B. F. Lasinski, J. Johnson, M. D. Perry, and E. M. Campbell, Phys. Rev. Lett. **85**, 2945 (2000).
[10] S. P. Hatchett, C. G. Brown, T. E. Cowan, E. A. Henry, J. S. Johnson, M. H. Key, J. A. Koch, A. B. Langdon, B. F. Lasinski, R. W. Lee, A. J. Mackinnon, D. M. Pennington, M. D. Perry, T. W. Phillips, M. Roth, T. C. Sangster, M. S. Singh, R. A. Snavely, M. A. Stoyer, S. C. Wilks, and K. Yasuike, Phys. Plasmas **7**, 2076 (2000).
[11] G. M. Petrov, D. P. Higginson, J. Davis, T. B. Petrova, J. M. McNaney, C. McGuffey, B. Qiao, and F. N. Beg, Phys. Plasmas **19**, 093106 (2012).
[12] A. Alejo, A. G. Krygier, H. Ahmed, J. T. Morrison, R. J. Clarke, J. Fuchs, A. Green, J. S. Green, D. Jung, A. Kleinschmidt, Z. Najmudin, H. Nakamura, P. Norreys, M. Notley, M. Oliver, M. Roth, L. Vassura, M. Zepf, M. Borghesi, R. R. Freeman, and S. Kar, Plasma Phys. Controlled Fusion **59**, 064004 (2017).
[13] Hui Chen, S. C. Wilks, J. D. Bonlie, E. P. Liang, J. Myatt, D. F. Price, D. D. Meyerhofer, and P. Beiersdorfer, Phys. Rev. Lett. **102**, 105001 (2009).
[14] Hui Chen, F. Fiuza, A. Link, A. Hazi, M. Hill, D. Hoarty, S. James, S. Kerr, D. D. Meyerhofer, J. Myatt, J. Park, Y. Sentoku, and G. J. Williams, Phys. Rev. Lett. **114**, 215001 (2015).
[15] D. J. Hoarty, P. Allan, S. F. James, C. R. D. Brown, L. M. R. Hobbs, M. P. Hill, J. W. O. Harris, J. Morton, M. G. Brookes, R. Shepherd, J. Dunn, H. Chen, E. Von Marley, P. Beiersdorfer, H. K. Chung, R. W. Lee, G. Brown, and J. Emig, Phys. Rev. Lett. **110**, 265003 (2013).
[16] A. McKelvey, G. E. Kemp, P. A. Sterne, A. Fernandez-Panella, R. Shepherd, M. Marinak, A. Link, G. W. Collins, H. Sio, J. King, R. R. Freeman, R. Hua, C. McGuffey, J. Kim, F. N. Beg, and Y. Ping, Sci. Rep. **7**, 7015 (2017).
[17] M. A. Purvis, V. N. Shlyaptsev, R. Hollinger, C. Bargsten, A. Pukhov, A. Prieto, Y. Wang, B. M. Luther, L. Yin, S. Wang, and J. J. Rocca, Nat. Photonics **7**, 796 (2013).
[18] A. Pukhov and J. Meyer-ter-Vehn, Phys. Rev. Lett. **76**, 3975 (1996).
[19] H. Xu, Z.-M. Sheng, J. Zhang, and X.-T. He, Phys. Scr. **77**, 045502 (2008).
[20] B. S. Paradkar, M. S. Wei, T. Yabuuchi, R. B. Stephens, M. G. Haines, S. I. Krasheninnikov, and F. N. Beg, Phys. Rev. E **83**, 046401 (2011).
[21] A. J. Kemp and L. Divol, Phys. Rev. Lett. **109**, 195005 (2012).
[22] A. P. L. Robinson, A. V. Arefiev, and D. Neely, Phys. Rev. Lett. **111**, 065002 (2013).
[23] A. Sorokovikova, A. V. Arefiev, C. McGuffey, B. Qiao, A. P. L. Robinson, M. S. Wei, H. S. McLean, and F. N. Beg, Phys. Rev. Lett. **116**, 155001 (2016).
[24] D. Wu, S. Krasheninnikov, S. Luan, and W. Yu, Nucl. Fusion **57**, 016007 (2016).
[25] J. Kim, A. J. Kemp, S. C. Wilks, D. H. Kalantar, S. Kerr, D. Mariscal, F. N. Beg, C. McGuffey, and T. Ma, Phys. Plasmas **25**, 083109 (2018).
[26] Y. Arikawa, S. Kojima, A. Morace, S. Sakata, T. Gawa, Y. Taguchi, Y. Abe, Z. Zhang, X. Vaisseau, S. H. Lee, K. Matsuo, S. Tosaki, M. Hata, K. Kawabata, Y. Kawakami, M. Ishida, K.

Tsuji, S. Matsuo, N. Morio, T. Kawasaki *et al.*, Appl. Opt. **55**, 6850 (2016).

[27] D. Batani, M. Koenig, J. L. Miquel, J. E. Ducret, E. d'Humieres, S. Hulin, J. Caron, J. L. Feugeas, P. Nicolai, V. Tikhonchuk, L. Serani, N. Blanchot, D. Raffestin, I. Thfoin-Lantuejoul, B. Rosse, C. Reverdin, A. Duval, F. Laniesse, A. Chancé, D. Dubreuil *et al.*, Phys. Scr. **2014**, 014016 (2014).

[28] L. J. Waxer, D. N. Maywar, J. H. Kelly, T. J. Kessler, B. E. Kruschwitz, S. J. Loucks, R. L. McCrory, D. D. Meyerhofer, S. F. B. Morse, C. Stoeckl, and J. D. Zuegel, Opt. Photon. News **16**, 30 (2005).

[29] J. M. Di Nicola, S. T. Yang, C. D. Boley, J. K. Crane, J. E. Heebner, T. M. Spinka, P. Arnold, C. P. J. Barty, M. W. Bowers, T. S. Budge, K. Christensen, J. W. Dawson, G. Erbert, E. Feigenbaum, G. Guss, C. Haefner, M. R. Hermann, D. Homoelle, J. A. Jarboe, J. K. Lawson *et al.*, Proc. SPIE **9345**, 93450I (2015).

[30] M. L. Spaeth, K. R. Manes, D. H. Kalantar, P. E. Miller, J. E. Heebner, E. S. Bliss, D. R. Spec, T. G. Parham, P. K. Whitman, P. J. Wegner, P. A. Baisden, J. A. Menapace, M. W. Bowers, S. J. Cohen, T. I. Suratwala, J. M. D. Nicola, M. A. Newton, J. J. Adams, J. B. Trenholme, R. G. Finucane *et al.*, Fusion Sci. Technol. **69**, 25 (2016).

[31] Hui Chen, M. R. Hermann, D. H. Kalantar, D. A. Martinez, P. D. Nicola, R. Tommasini, O. L. Landen, D. Alessi, M. Bowers, D. Browning, G. Brunton, T. Budge, J. Crane, J.-M. D. Nicola, T. Döppner, S. Dixit, G. Erbert, B. Fishler, J. Halpin, M. Hamamoto *et al.*, Phys. Plasmas **24**, 033112 (2017).

[32] R. Tommasini, C. Bailey, D. K. Bradley, M. Bowers, H. Chen, J. M. D. Nicola, P. D. Nicola, G. Gururangan, G. N. Hall, C. M. Hardy, D. Hargrove, M. Hermann, M. Hohenberger, J. P. Holder, W. Hsing, N. Izumi, D. Kalantar, S. Khan, J. Kroll, O. L. Landen *et al.*, Phys. Plasmas **24**, 053104 (2017).

[33] S. Kojima, Y. Arikawa, A. Morace, M. Hata, H. Nagatomo, T. Ozaki, S. Sakata, S. H. Lee, K. Matsuo, K. F. F. Law, S. Tosaki, A. Yogo, T. Johzaki, A. Sunahara, H. Sakagami, M. Nakai, H. Nishimura, H. Shiraga, S. Fujioka, and H. Azechi, J. Phys.: Conf. Ser. **717**, 012102 (2016).

[34] A. Yogo, K. Mima, N. Iwata, S. Tosaki, A. Morace, Y. Arikawa, S. Fujioka, T. Johzaki, Y. Sentoku, H. Nishimura, A. Sagisaka, K. Matsuo, N. Kamitsukasa, S. Kojima, H. Nagatomo, M. Nakai, H. Shiraga, M. Murakami, S. Tokita, J. Kawanaka *et al.*, Sci. Rep. **7**, 42451 (2017).

[35] D. Rusby, R. Gray, N. Butler, R. Dance, G. Scott, V. Bagnoud, B. Zielbauer, P. McKenna, and D. Neely, EPJ Web Conf. **167**, 02001 (2018).

[36] J. Fuchs, P. Antici, E. d'Humieres, E. Lefebvre, M. Borghesi, E. Brambrink, C. A. Cecchetti, M. Kaluza, V. Malka, M. Manclossi, S. Meyroneinc, P. Mora, J. Schreiber, T. Toncian, H. Pepin, and P. Audebert, Nat. Phys. **2**, 48 (2006).

[37] J. Myatt, J. A. Delettrez, A. V. Maximov, D. D. Meyerhofer, R. W. Short, C. Stoeckl, and M. Storm, Phys. Rev. E **79**, 066409 (2009).

[38] G. J. Williams, D. Barnak, G. Fiksel, A. Hazi, S. Kerr, C. Krauland, A. Link, M. J.-E. Manuel, S. R. Nagel, J. Park, J. Peebles, B. B. Pollock, F. N. Beg, R. Betti, and H. Chen, Phys. Plasmas **23**, 123109 (2016).

[39] See Supplemental Material at http://link.aps.org/supplemental/10.1103/PhysRevE.101.031201 for additional details of experimental geometry and laser parameters.

[40] Hui Chen, A. J. Link, R. van Maren, P. K. Patel, R. Shepherd, S. C. Wilks, and P. Beiersdorfer, Rev. Sci. Instrum. **79**, 10E533 (2008).

[41] F. N. Beg, A. R. Bell, A. E. Dangor, C. N. Danson, A. P. Fews, M. E. Glinsky, B. A. Hammel, P. Lee, P. A. Norreys, and M. Tatarakis, Phys. Plasmas **4**, 447 (1997).

[42] C. Thoma, D. R. Welch, R. E. Clark, D. V. Rose, and I. E. Golovkin, Phys. Plasmas **24**, 062707 (2017).

[43] Y. T. Lee and R. M. More, Phys. Fluids **27**, 1273 (1984).

[44] M. P. Desjarlais, Contrib. Plasma Phys. **41**, 267 (2001).

[45] S. Atzeni, A. Schiavi, and J. R. Davies, Plasma Phys. Controlled Fusion **51**, 015016 (2009).

[46] J. A. Halbleib, R. P. Kensek, G. D. Valdez, S. M. Seltzer, and M. J. Berger, IEEE Trans. Nucl. Sci. **39**, 1025 (1992).

[47] M. M. Marinak, G. D. Kerbel, N. A. Gentile, O. Jones, D. Munro, S. Pollaine, T. R. Dittrich, and S. W. Haan, Phys. Plasmas **8**, 2275 (2001).

[48] C. S. Brady, A. Lawrence-Douglas, and T. D. Arber, Phys. Plasmas **19**, 063112 (2012).

[49] T. Nakamura, S. Kato, M. Tamimoto, and T. Kato, Phys. Plasmas **9**, 1801 (2002).

[50] S. G. Bochkarev, A. V. Brantov, V. Y. Bychenkov, D. V. Torshin, V. F. Kovalev, G. V. Baidin, and V. A. Lykov, Plasma Phys. Rep. **40**, 202 (2014).

[51] J. Allison, K. Amako, J. Apostolakis, H. Araujo, P. Dubois, M. Asai, G. Barrand, R. Capra, S. Chauvie, R. Chytracek, G. Cirrone, G. Cooperman, G. Cosmo, G. Cuttone, G. Daquino, M. Donszelmann, M. Dressel, G. Folger, F. Foppiano, J. Generowicz *et al.*, IEEE Trans. Nucl. Sci. **53**, 270 (2006).

[52] A. Link, R. R. Freeman, D. W. Schumacher, and L. D. Van Woerkom, Phys. Plasmas **18**, 053107 (2011).